Effects of the Compatibilizer Structural Parameters on Microstructural Formation in Ethylene–Propylene–Diene Monomer Rubber/Ethylene–Propylene–Diene Monomer Rubber-*g*-Maleic Anhydride/Organoclay Nanocomposites

Y. Mohammadpour, A. A. Katbab

Polymer Engineering Department, Amirkabir University of Technology, Tehran, Iran

Received 5 May 2009; accepted 29 August 2010
DOI 10.1002/app.33327
Published online 10 February 2011 in Wiley Online Library (wileyonlinelibrary.com).

ABSTRACT: Nanocomposite vulcanizates based on ethylene–propylene–diene monomer rubber (EPDM) and organically modified montmorillonite with improved mechanical and barrier properties were prepared via a melt-mixing process in the presence of maleic anhydride grafted ethylene–propylene–diene monomer rubber (EPDM-*g*-MAH) as an interfacial compatibilizer. The effects of the EPDM Mooney viscosity as the matrix and also the compatibilizer molecular weight and its maleation degree on the developed microstructure were also studied. The annealing of the vulcanized nanocomposites based on a low-Mooney-viscosity EPDM matrix and low-Mooney-viscosity EPDM-*g*-MAH enhanced the flocculation of the dispersed clay platelets; this implied that the flocculated structure for the clay nanolayers was more thermodynamically preferred in these nanocomposites. This was verified by the decrease in the oxygen permeability of the nanocomposite vulcanizates with increasing annealing time. The tendency of the clay nanosilicate layers to flocculate within the matrix of EPDM was found to be influenced by the clay volume fraction, the maleation degree, and also, the Mooney viscosity of the compatibilizer. Interfacially compatibilized nanocomposites based on high-molecular-weight EPDM exhibited a more disordered dispersion of the clay nanolayers, with a broadened relaxation time spectra; this was attributed to the higher shearing subjected to the mix during the melt-blending process. © 2011 Wiley Periodicals, Inc. J Appl Polym Sci 120: 3133–3140, 2011

Key words: compatibilization; microstructure; polyolefins

INTRODUCTION

Polymer nanocomposites (organic/inorganic hybrids) have attracted great academic and industrial interest during recent decades because of their superior properties, including their light weight, excellent barrier performance, high heat distortion temperature, and enhanced mechanical properties at low nanofiller contents.[1–8] The unexpected beneficial behavior of nanocomposites is mainly attributed to the high filler/matrix and filler/filler interactions as a result of their ultrahigh surface-to-volume ratio, which is provided by the well-dispersed nanosized particles. However, to achieve efficient property improvement in polymer/clay nanocomposites, the *d*-spacing between the silicate nanolayers should be made accessible to the polymer chains. All of the properties of this important class of materials are controlled by their microstructure, which is governed by several parameters, including the type of material, the processing conditions, and the extent of interaction between the nanoparticles and the polymer matrix. Among various possible methods, melt intercalation has received great attention.[9–15] However, to enhance the intercalation between the clay silicate nanolayers and nonpolar polymers, such as ethylene–propylene–diene monomer rubber (EPDM), the incorporation of a functionalized compatibilizer, such as maleic anhydride grafted ethylene–propylene–diene monomer rubber (EPDM-*g*-MAH), into the material recipe facilitates the interdiffusion of the polymer chains into the gallery spaces of the nanoclay. Montmorillonite/EPDM nanocomposites have been prepared by the melt-mixing method, and the effects of the vulcanization system on the developed microstructure have also been investigated.[8] The degree of interaction between EPDM rubber and organoclay particles during the melt-mixing process is mainly controlled by EPDM microstructural parameters, such as the molecular weight (Mooney viscosity) and ethylene content, and also the structural parameters of the compatibilizer, such as the degree of maleation and the melt viscosity.

In this study, we attempted to investigate the effects of the EPDM Mooney viscosity and the structural parameters of EPDM-*g*-MAH as a compatibilizer on the

Correspondence to: A. A. Katbab (katbab@aut.ac.ir).

TABLE I
Characteristics of the EPDMs Used as the Matrices

EPDM grade	ML(1 + 4), 125°C	Ethylene content (%)	Linearity	Supplier	Diene type
Keltan 2340A	25	54	Controlled long-chain branching	DSM (Holland, Heerlen)	ENB
Keltan 8340A	85	54	Controlled long-chain branching	DSM (Holland, Heerlen)	ENB

microstructure of EPDM/EPDM-*g*-MAH/organoclay nanocomposites. The influence of the annealing process on the nanocomposite microstructure and oxygen gas permeability were also studied.

EXPERIMENTAL

Materials

Two different grades of EPDM rubber with the characteristics given in Table I were used as the composite matrices. Two types of EPDM-*g*-MAH, with the trade names OPTIM P-635 and OPTIM P-468, with maleic anhydride (MAH) contents of 0.4 and 1.2 wt %, respectively, were supplied by Pluss Polymers Pvt., Ltd. (New Delhi, India). The Mooney viscosity of these two OPTIMs was ML (1+4) 125°C = 22. High-molecular-weight EPDM-*g*-MAH, with an MAH content of 0.4 wt % and a Mooney viscosity of M(L1+4) 125°C = 80, was synthesized in our laboratory. The organoclay [organically modified montmorillonite (o-MMT)] that we used was montmorillonite modified by dimethyl dehydrogenated tallow ammonium with the commercial name Dellite 67G and was provided by Laviosa Chemica Mineraria S. p. A (Livorno, Italy). A sulfur curing system with the recipe given in Table II was used for the vulcanization of the prepared compounds.

Preparation of the EPDM/clay composite samples

Different EPDM/o-MMT and EPDM/EPDM-*g*-MAH/o-MMT composites were prepared by a melt-compounding process with the compositions given in Table III. EPDM-*g*-MAH was first melt-mixed with o-MMT in a Banbury-type internal mixer (Haake Buchler HBI system 90, Sattle Brook, NJ) at 180°C and at a rotor speed of 60 rpm. EPDM-*g*-MAH was first fed into the mixer, and o-MMT was incorporated after 1 min. Mixing was continued until the mixing torque was stabilized. The prepared master batch was removed and mixed with the desired EPDM rubber in a laboratory-size two-roll mill (Farrel Bridge, London, UK) at a temperature of 60°C for 10 min. The curing ingredients were then added, and compounding was continued for another 3 min.

The prepared compounds were vulcanized at 165°C into films with thicknesses of 2.5–3 mm. The curing time for different composite samples was determined on the basis of the optimum cure read from the curing rheograph obtained for each compound with a Monsanto rubber rheometer (model 100S, London, UK). All of the prepared samples were coded as illustrated in Table III.

Characterization techniques

X-ray diffraction (XRD) patterns of the samples were obtained with an Expert Philips (Hamburg, Germany) X-ray diffractometer in reflection mode with Ni-filtered Cu Kα radiation (λ = 0.154056 nm) at a generator voltage of 30 kV and a current of 30 mA. Samples were scanned in step mode within the range 1.5–10°. The microstructure of the prepared samples was also examined with a JEOL/200 EXII (Tokyo, Japan) transmission electron microscope under an acceleration voltage of 120 kV. Specimens for transmission electron microscopy (TEM) examination were prepared with an ultrahigh cryomicrotome.

The mechanical properties of the composite samples were evaluated with a tensile tester (Monsanto T500, London, UK) at 25°C with a crosshead speed of 500 mm/min. For this purpose, dumbbell-shaped specimens with dimensions according to the ASTM D 412 were die-cut from compression-molded sheets.

The linear melt viscoelastic behavior of the samples was studied with a rheometric mechanical spectrometer (Paar Physica US200, Austria, Graz) with a set of parallel plates 25 mm in diameter with a gap of 1 mm at 180°C. The dynamic strain sweep was first conducted at 1 rad/s and 0.1–100 strain to determine the strain region where the linear behavior was retained.

Thermogravimetric analysis (TGA) was also performed to evaluate the thermal behavior of the samples with a DuPont thermogravimetric analyzer (model 951, Austin, TX), and thermograms were

TABLE II
Components of the Vulcanizing System Used

Ingredient	Phr
EPDM + EPDM-*g*-MAH	100
ZnO	5
Stearic acid	1.5
MBT (Mercapto Benzo Thiazole)	0.9
CZ (Cyclohexyl Benzo Thiazole-2 Sulfenamide)	0.7
Sulfur	1.5

TABLE III
Samples and Compositions of the Prepared Composites

Code	Compatibilizer Type	Compatibilizer %	o-MMT (%)	EPDM type
200	–	0	0	Keltan 2340A
800	–	0	0	Keltan 8340A
250	–	0	5	Keltan 2340A
850	–	0	5	Keltan 8340A
255H	Laboratory made	5	5	Keltan 2340A
255L	OPTIM P-635	5	5	Keltan 2340A
255P	OPTIM P-468	5	5	Keltan 2340A
855L	OPTIM P-635	5	5	Keltan 8340A
2515L	OPTIM P-635	15	5	Keltan 2340A
8515L	OPTIM P-635	15	5	Keltan 8340A
8515H	Laboratory made	15	5	Keltan 8340A

obtained in the presence of air at a heating rate of 10°C/min according to ASTM E 2105.

Annealing was performed on some of the vulcanized nanocomposite samples at 90°C for 48 h. The samples were then dried on filter paper and weighted after 1 min.

To obtain further information about the microstructure, the oxygen gas permeabilities of the samples were evaluated at 20°C and 90% relative humidity with a GDP-C 150 gas permeability tester (Munich, Germany) according to ASTM D 1434. For this purpose, vulcanized test samples with a thickness of about 200 μm were prepared by a hot-press compression-molding process at 165°C. To measure the permeability, oxygen with a stream of 100 cm^3/min was imposed on one side of the test sample, which was kept *in vacuo* for 15 min in the test chamber, and then, the permeability was read when the OTR (Oscillating Torque Rheometer) curve reached the steady state.

RESULTS AND DISCUSSION

Microstructure studies

Microstructural characterization was carried out for the samples prepared with different compositions. Because of the lamellar structure of o-MMT, XRD was used as a powerful technique for monitoring the structure and extent of intercalation. Figure 1 illustrates the XRD spectra of the pristine o-MMT along with the XRD scans of the as-prepared composites based on high- and low-Mooney-viscosity EPDM matrices and low-Mooney-viscosity EPDM-*g*-MAH with 0.4 wt % maleation. The neat o-MMT showed diffraction peaks around $2\theta = 6.8$, 4.2, and 2.8 corresponding to basal spacings of $d_{003} = 1.30$ nm, $d_{002} = 1.94$ nm, and $d_{001} = 3.3$ nm, respectively. The two low-spacing diffraction peaks were related to the clay tactoids, which were weakly modified by the surfactant, and the main characteristic peak of the organoclay used, which was involved in the intercalation of the polymer, was located at $2\theta = 2.8$. It was clear that the main diffraction peaks of o-MMT were not removed in the structure of the uncompatibilized composites based on the low- and high-Mooney-viscosity EPDM rubber (samples 250 and 850) but only showed a slight shift to the lower angles for the sample originated from EPDM with a low Mooney viscosity (sample 250). This indicated easier diffusion of the low-molecular-weight EPDM into the galleries of o-MMT. The incorporation of low-Mooney-viscosity EPDM-*g*-MAH with a maleation content of 0.4% (OPTIM p-635) as a compatibilizer resulted in enhanced intercalation and exfoliation of the clay nanolayers. However, the interfacially compatibilized EPDM/EPDM-*g*-MAH/o-MMT nanocomposites based on the high-Mooney-viscosity EPDM matrix (sample 8515L) showed a higher extent of disordered dispersion; this was attributed to the higher melt viscosity of the mix and, consequently, the more intensive shearing of the intercalated clay particles. When clay tactoids are intercalated by polymer segments, which occurs preferentially with d_{001} spacing rather than with d_{002} and d_{003} spacing, the 1 : 2 : 3 rule for the clay diffraction peaks might not be obeyed anymore. The main reason is that interdiffusion of polymer chains into the three *d*-spacings does not happen to a similar extent.

Figure 2 demonstrates the XRD patterns of the nanocomposites based on the high- and low-molecular-weight EPDM matrices and the high-Mooney-viscosity EPDM-*g*-MAH as a compatibilizer (samples 255H and 8515H, respectively). Clearly, none of the o-MMT peaks disappeared, but they shifted to lower diffraction angles; this implied a mainly intercalation microstructure. These results imply that the low-

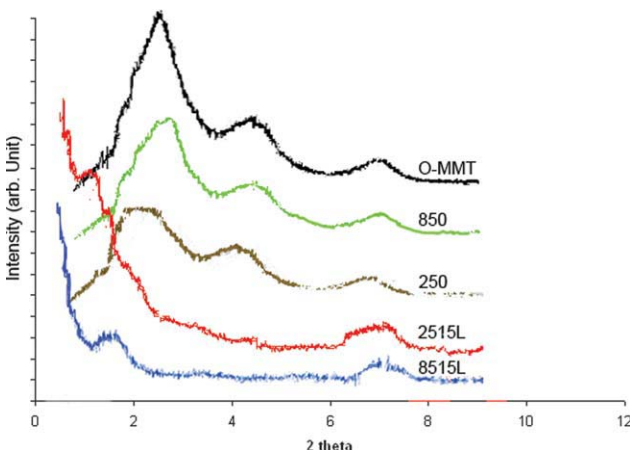

Figure 1 XRD patterns of the EPDM/o-MMT nanocomposite based on high- and low-Mooney-viscosity EPDM matrices and low-Mooney EPDM-*g*-MAH with 0.4 wt % maleation (OPTIM P-635) as a compatibilizer. [Color figure can be viewed in the online issue, which is available at wileyonlinelibrary.com.]

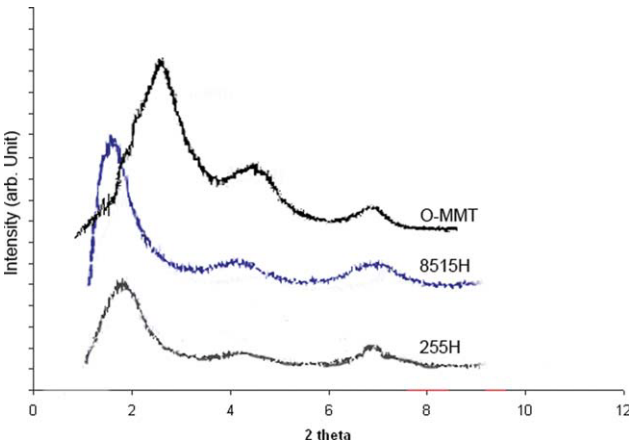

Figure 2 XRD patterns of the EPDM/o-MMT nanocomposites based on the high- and low-Mooney-viscosity EPDM matrices and high-Mooney EPDM-*g*-MAH with 0.4 wt % maleation (OPTIM P-635) as a compatibilizer. [Color figure can be viewed in the online issue, which is available at wileyonlinelibrary.com.]

Mooney-viscosity EPDM-*g*-MAH enhanced the diffusion of the EPDM macromolecular chains into the clay galleries, regardless of the matrix Mooney viscosity. These were consistent with the TEM micrographs, as thinner clay platelets appeared in the microstructure of sample 2515L compared with the 8515L nanocomposite (Fig. 3). Increasing the level of maleation in the low-Mooney EPDM-*g*-MAH also led to better dispersion of the clay platelets as a result of enhanced interfacial interaction. This was confirmed by a comparison of the TEM micrographs of the two 255L and 2515L nanocomposites based on low-Mooney-viscosity EPDM matrices composed of 5 and 15 wt % low-Mooney-viscosity compatibilizer, respectively, with 0.4 wt % maleation. The presence of high-length nanolayers in the microstructure of 255L [Fig. 3(a)] was evidence for the flocculation of nanoplatelets as a result of weak dispersion and, therefore, a low interparticle distance compared with the 2515L nanocomposite. This was consistent with the lower oxygen permeability exhibited by the 255L sample, as presented in Table IV.

Dynamic melt rheological behavior

Dynamic melt rheological study has been found to be a powerful means for evaluating the microstructure of polymer/filler nanocomposites and for investigating the possible formation of physical networks by nanofiller particles. Therefore, the elucidation of the melt rheology is correlated to the microstructural observation. Figures 4 and 5 show the variations of the dynamic elastic storage modulus (G') and loss modulus (G'') versus the frequency for the different samples in the molten state. For all of samples, G' and G'' increased with frequency; this was attributed to insufficient time for chain relaxation within the high-frequency region.[2,16] Moreover, all of the composite samples exhibited higher melt elastic modulus than their neat EPDM matrix with nonterminal behavior within the low-frequency region; this indicated high interaction between the clay platelets and the EPDM matrix. This is evidenced in figure 6 as the retardation time spectrum, $H(\lambda)$, Showed to be wider than that of the neat EPDM. Comparing the G' versus frequency plots of the nanocomposites based on high-viscosity EPDM and low-viscosity EPDM-*g*-MAH (samples 855L and 8515L) with that of nanocomposites generated from the low-viscosity matrix (sample 255L and 2515L), we observed more pseudo-solid-like and nonterminal characteristics for the 2515L sample. This indicated more restricted motion for the EPDM chains because of the higher interfacial surface between the EPDM chains and o-MMT particles in the 255L and 2515L nanocomposites; this was consistent with the XRD and TEM results. As shown in Figure 4(c), the nanocomposite prepared by the low-viscosity EPDM matrix and low-viscosity EPDM-*g*-MAH with maleation content of 0.4 wt % exhibited a higher melt elasticity with more pseudo-solid-like behavior than the counterpart sample containing low-viscosity EPDM-*g*-MAH but with a maleation content of 1.2 wt %. This implied that high-functionalized EPDM-*g*-MAH was not able to enhance the interdiffusion of EPDM segments into the clay galleries because of the increased polarity and, hence, less thermodynamic affinity for the EPDM chains to reside between the clay nanolayers.

Thermal behavior

The nonisothermal weight loss curves obtained from TGA of the different EPDM/O-MMT composites are presented in Figure 7. The neat EPDM, sample 200, showed a very sharp weight loss between 375 and 425°C followed by a short step near 500°C, whereas the nanocomposite samples showed small gradual weight losses above 200°C with a higher degradation temperature; this implied enhanced thermal resistance by the EPDM/O-MMT nanocomposites. Improved thermal resistance was clearly observed for the interfacially compatibilized samples (2515 and 255) generated from the low-molecular-weight EPDM matrix, 5 wt % o-MMT, and 5 and 15 wt % low-Mooney-viscosity EPDM-*g*-MAH, respectively. This was attributed to thermal shielding effects imparted by the dispersed clay nanolayers.

The weight loss rate (slope of the weight loss curve) for the nanocomposites composed of low-Mooney-viscosity EPDM-*g*-MAH was lower than that of the corresponding neat EPDM, and the onset of thermal degradation was improved by 40°C. This improvement in thermal stability was related to the presence of impenetrable silicate layers with a large

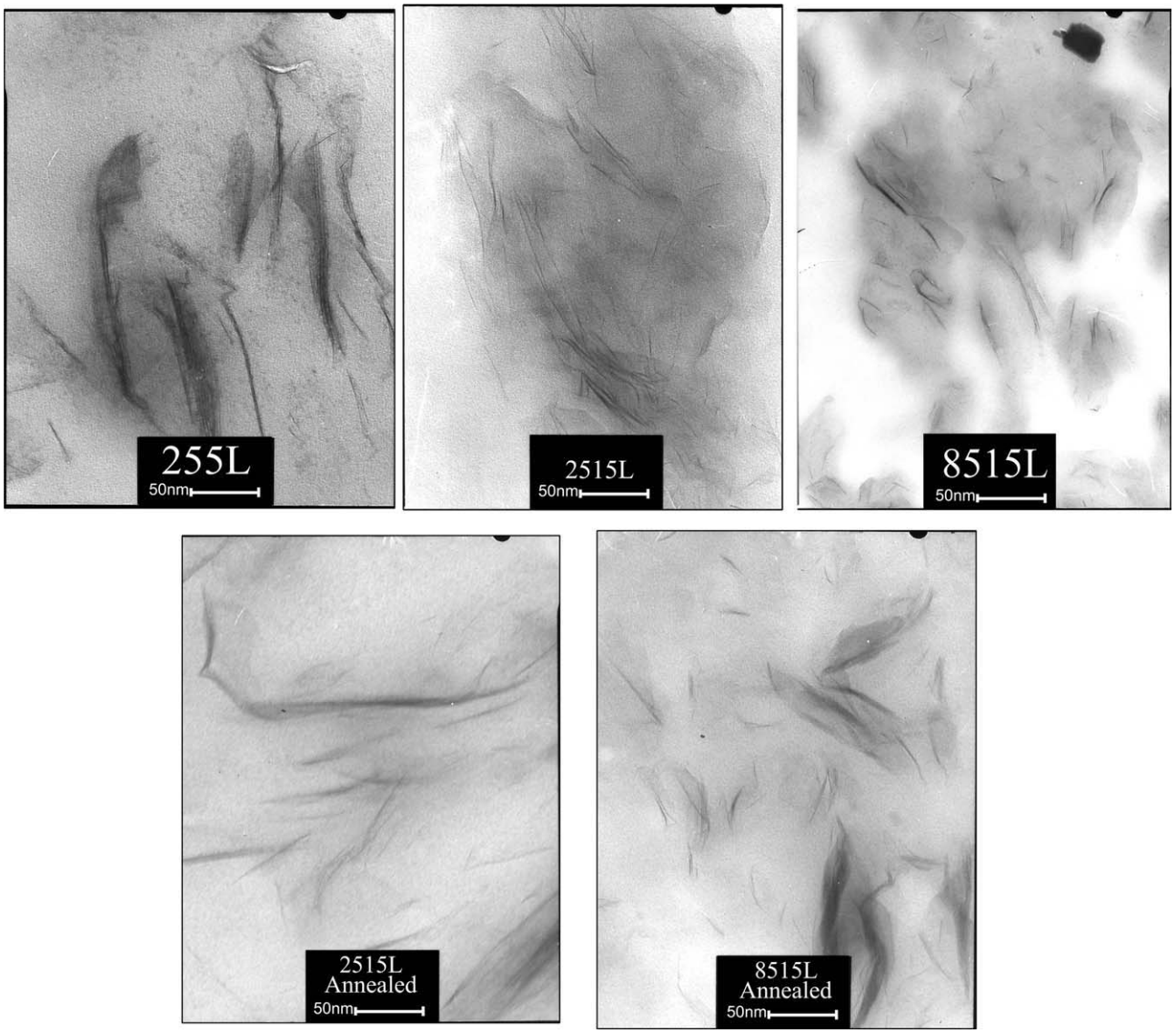

Figure 3 TEM micrographs of the vulcanized EPDM/o-MMT nanocomposite samples composed of 5 and 15 wt % low-Mooney compatibilizers (OPTIM p-635): (a) samples 255L, 2515L, and 8515L and (b) annealed samples 2515L and 8515L.

aspect ratio, which offered a great barrier effect to hinder the migration of small molecules resulting from thermal decomposition to the surface.[8] These layers could also decrease the heat flow in the samples.[7] Sirivastaka et al.[17] also believed that the coexistence of intercalated and exfoliated silicate layers in the EPDM matrix, which increased the Si—O—C interfacial interaction to restrict the thermal motion of EPDM polymer segments, was another possibility.

Oxygen gas permeability

The incorporation of layered structure nanofillers into polymer matrices has been shown to be highly effective in reducing gas and solvent permeability.[2,18] This has been attributed to the formation of a torturous path by the dispersed nanolayers. In Table IV, the oxygen gas permeability values for different prepared EPDM/o-MMT composites based on low- and high-molecular-weight EPDM rubber are shown. The

TABLE IV
O_2 Gas Permeation Values for Different Vulcanized Samples

Sample	800	855L	8515L	200	2515L	255L	Annealed 2515L	Annealed 8515L
Permeation ($cm^3\ m^{-1}\ day^{-1}\ bar^{-1}$)	585	461	315	630	510	580	320	280

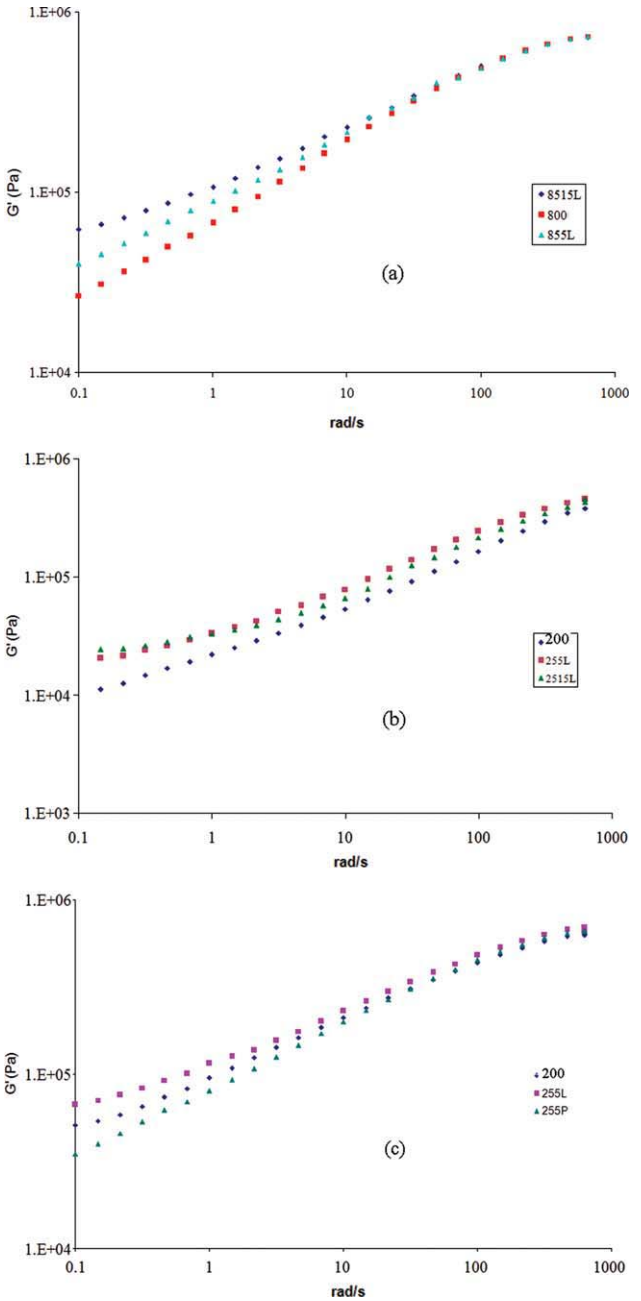

Figure 4 Plots of the dynamic melt G' at 190°C for various neat EPDM and the corresponding composites. [Color figure can be viewed in the online issue, which is available at wileyonlinelibrary.com.]

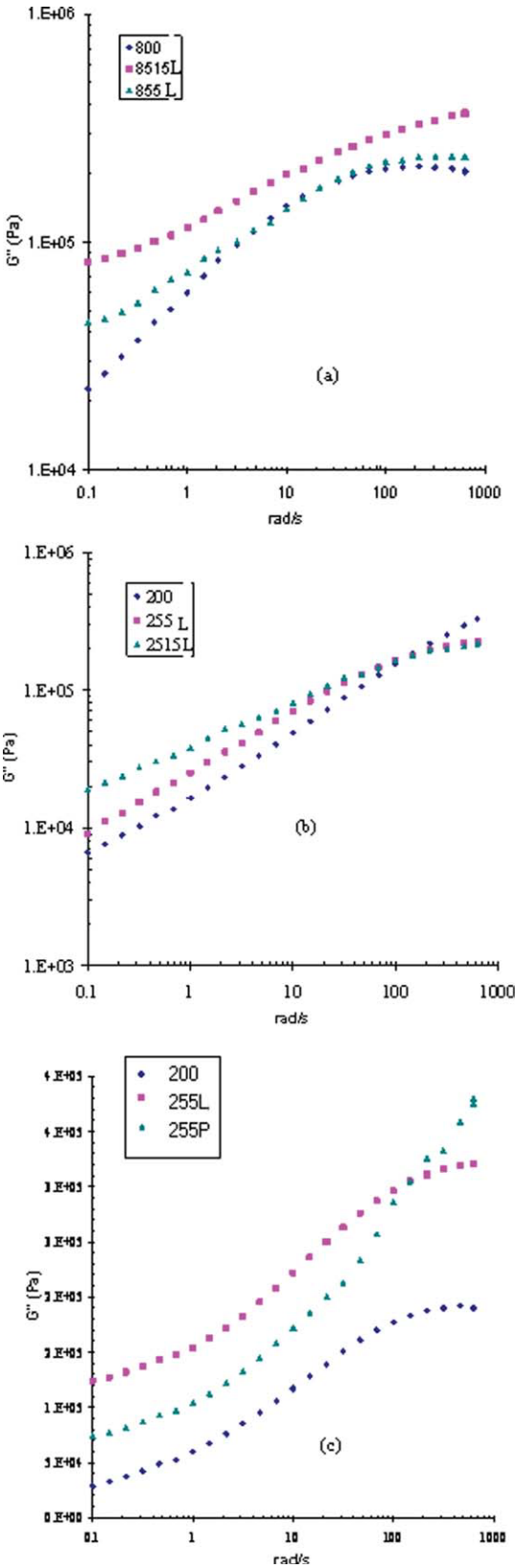

Figure 5 Plots of the dynamic melt G' at 190°C for various neat EPDMs and the corresponding composites. [Color figure can be viewed in the online issue, which is available at wileyonlinelibrary.com.]

presence of silicate layers in the EPDM matrix led to a decrease in the oxygen gas permeability. However, all of the composite samples prepared by the high-Mooney-viscosity EPDM (code 8) showed lower permeability, even with a low content of interfacial compatibilizer. The best barrier properties were shown by sample 8515L, which was based on the high-viscosity EPDM matrix and 15 wt % low-Mooney-viscosity EPDM-*g*-MAH as a compatibilizer; this was consistent with the XRD and TEM analysis results observed for samples 8515L, shown in Figures 1 and 3(a).

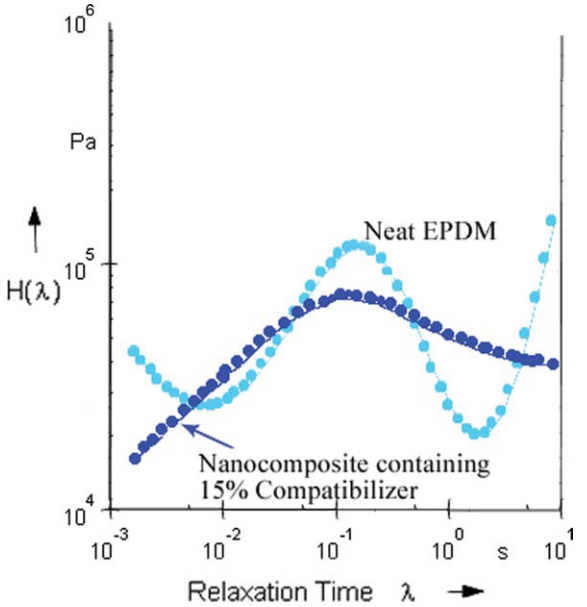

Figure 6 Comparison between the retardation time spectrum, H(λ), of the neat high-Mooney EPDM (8340A) and corresponding nanocomposite (sample 8518L) composed of 5% nanoclay and 15 wt % low-Mooney EPDM-*g*-MAH (OPTIM 635). [Color figure can be viewed in the online issue, which is available at wileyonlinelibrary.com.]

Tensile properties

The most important feature of polymer/clay nanocomposites is the remarkable improvement in their mechanical properties, such as in the tensile strength and modulus. There are several parameters that can influence the mechanical properties of a polymer/clay nanocomposite, including the extent of interaction between the clay and polymer matrix, the state of dispersion, and the aspect ratio.[8] The measured tensile properties of the prepared nanocomposite samples are illustrated in Table V and were compared with their corresponding neat EPDM vulcanizates. We observed that the tensile modulus of the samples containing o-MMT was enhanced significantly. The tensile modulus of samples 255H and 2515L were about 50 and 300% higher than that of sample 200. This was attributed to the large and intensified interface between the matrix and nanolayers, which led to a higher stiffness. The higher enhancement in the tensile properties for sample 2515L was in good agreement with its XRD patterns.

The tensile modulus of the samples with a high-viscosity matrix and different compatibilizers showed that the compatibilizer with a lower Mooney viscosity and low maleation content was more successful in modulus enhancement. This means that the microstructure of the nanocomposite samples was one of the most important parameters in mechanical property improvement.

Annealing process

Figure 3(b) demonstrates the TEM micrographs of the nanocomposite samples 2515L and 8515L, which

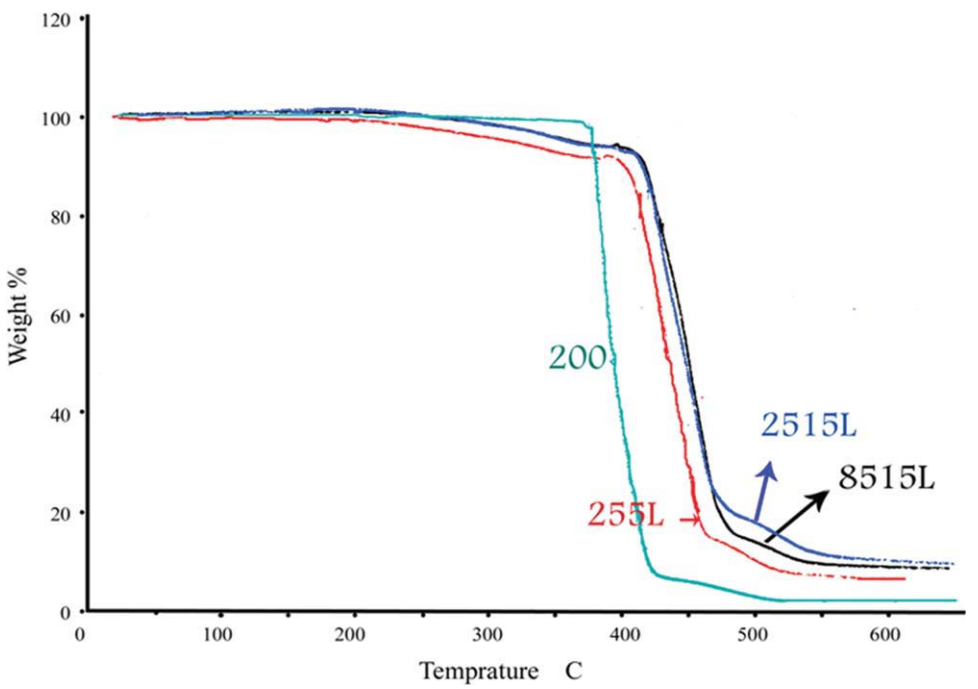

Figure 7 TGA thermograms of the neat low-Mooney-viscosity EPDM (sample 200) and its corresponding composite based on OPTIM 635 with a low-Mooney-viscosity matrix (samples 2515L and 255L) and with a high-Mooney-viscosity matrix (sample 8515L). [Color figure can be viewed in the online issue, which is available at wileyonlinelibrary.com.]

TABLE V
Tensile Mechanical Properties of the Neat EPDM Vulcanizate and Corresponding Composite Vulcanizates

Sample	Tensile modulus (MPa)	Tensile strength (MPa)	Elongation at break (%)
200	1.2	2.1	300
800	1.3	2.4	270
250	1.4	2.6	210
850	1.5	2.3	280
255H	2.1	4.4	230
255L	2.0	4.1	250
255P	2.2	3.3	190
855L	2.4	4.8	220
2515L	3.2	5.3	330
Annealed 2515L	3.9	5.7	385
8515L	3.9	6.8	310
Annealed 8515L	4.1	6.5	340
8515H	3.4	4.1	240

endured 48 h of annealing at 90°C. Compared with the TEM micrograph taken from the surface of these samples before annealing [Fig. 3(a)], more flocculation of the clay nanolayers was achieved after the annealing process in the microstructure of the 2515L samples based on the low-molecular-weight EPDM matrix (2340A) and low-Mooney-viscosity compatibilizer (optim-635) than in that of the sample generated from the high-molecular-weight EPDM matrix (8340A). This was consistent with the oxygen gas barrier properties and the tensile behavior of these samples, as presented in Tables IV and V, respectively.

The elastic modulus of the annealed sample 2515L showed a greater increase than the annealed 8515L sample. This was attributed to the higher aspect ratio for the clay nanolayers in the structure of the annealed 2515L nanocomposite, which led to a higher interacting surfaces with the matrix and more mechanical enhancement.[8] Therefore, the enhanced thermal motion of the polymer chains during the annealing process provided a better chance for the silicate layers to move toward each other; leading to their flocculation. Moreover, the silicate layers had more mobility within the low-viscosity EPDM matrix in sample 2515L.

CONCLUSIONS

Interfacially compatibilized EPDM/EPDM-*g*-MAH/o-MMT based on low- and high-molecular-weight EPDM matrices were prepared via a direct melt-mixing process. The role of the EPDM-*g*-MAH Mooney viscosity and the degree of maleation on the development of the microstructure, that is, the intercalation/exfoliation and flocculation of the clay nanolayers and their dispersion state were evaluated and correlated with the dynamic melt rheological behavior, oxygen permeability, and mechanical properties of the vulcanized nanocomposites. The results show that the low-Mooney-viscosity compatibilizer enhanced the extent of polymer/clay interactions, and hence, a higher degree of exfoliated structure occurred than when the high-Mooney-viscosity EPDM-*g*-MAH was used as a compatibilizer. The degree of clay nanolayer flocculation during the annealing process was found to be higher for the nanocomposites based on the low-Mooney-viscosity EPDM matrix and low-Mooney-viscosity compatibilizer; this led to enhanced barrier properties and tensile moduli. The EPDM-*g*-MAH with a low Mooney viscosity but a high content of MAH was shown to not be as effective in enhancing the intercalation of the EPDM matrix into the galleries of the o-MMT particles. This indicated that a low Mooney viscosity with a low maleation content was much more beneficial in the preparation of the EPDM/o-MMT nanocomposites with a high extent of exfoliation of the clay platelets, regardless of the molecular weight of the EPDM matrix. Moreover, the high-molecular-weight EPDM (8340A) was shown to impose more intensive shearing on the mix during the melt-blending process. This led to a more disordered arrangement of the clay nanolayers throughout the EPDM matrix.

References

1. Ahmadi, S. J.; Huang, Y.; Li, W. Compos Sci Technol 2005, 65, 1069.
2. Ray, S. S.; Okamoto, K.; Okamoto, M. Macromolecules 2003, 36, 2355.
3. Quang, T. N.; Baird, D. G. Adv Polym Technol 2006, 25, 270.
4. Kim, D. H.; Park, J. U.; Cho, K. S.; Ahn, K. H.; Lee, S. J. Macromol Mater Eng 2006, 291, 1127.
5. Ray, S. S.; Okamoto, M. Prog Polym Sci 2003, 28, 1539.
6. Fornes, T. D.; Yoon, P. J.; Keskkula, H.; Paul, D. R. Polymer 2001, 42, 9929.
7. Parija, S.; Nayak, S. K.; Verma, S. K.; Tripathy, S. S. Polym Compos 2004, 25, 646.
8. Mohammadpour, Y.; Katbab, A. A. J Appl Sci 2007, 106, 4209.
9. Fan, J.; Liu, S.; Chen, G.; Qi, Z. J Appl Polym Sci 2002, 83, 66.
10. Xia, H.; Zhang, C.; Wang, Q. J Appl Polym Sci 2001, 80, 1130.
11. Hwu, Z. W.; Zhou, C.; Qi, R.; Zhang, H. J Appl Polym Sci 2002, 83, 2403.
12. Jiang, J. G.; Gao, Z. M.; Xie, W.; Pan, W. P. J Appl Polym Sci 2002, 83, 1702.
13. Wu, Y. P.; Jia, Q. X.; Yu, D. S.; Zhang, L. Q. J Appl Polym Sci 2003, 89, 3855.
14. Ma, Y.; Wu, Y. P.; Wang, Y. Q.; Zhang, L. Q. J Appl Polym Sci 2006, 99, 914.
15. Loo, Y. L.; Register, R. A.; Ryan, A. J. Phys Rev Lett 2002, 25, 2365.
16. Dong, W.; Liu, Y.; Zhang, X.; Gao, J.; Huang, F.; Song, Z.; Tan, B.; Qiao, J. Macromolecules 2005, 38, 4551.
17. Acharya, H.; Pramanik, M.; Srivastava, S. K.; Bhowmick, A. K. J Appl Polym Sci 2004, 93, 2429.
18. Nilson, L. E.; Landel, R. F. Mechanical Properties of Polymers and Composites, 2nd ed.; Marcel Dekker: New York, 1994.